

MASTER

RECEIVED BY TIC MAR 12 1980

LBL-9813



# Lawrence Berkeley Laboratory

UNIVERSITY OF CALIFORNIA

## Engineering & Technical Services Division

Presented at the Course on Advances in Radiation, Lecture No. 10,  
International School of Radiation Damage and Protection, Ettore  
Majorana Centre for Scientific Culture, Erice, Italy,  
September 1979

PASSIVE DETECTORS

Ralph H. Thomas

September 1979



Prepared for the U.S. Department of Energy under Contract W-7405-ENG-48

DISTRIBUTION OF THIS DOCUMENT IS UNLIMITED

**DISCLAIMER**

This book was prepared as an account of work sponsored by an agency of the United States Government. Neither the United States Government nor any agency thereof, nor any of their employees, make any warranty, express or implied, or assumes any legal liability or responsibility for the accuracy, completeness, or usefulness of any information, apparatus, product, or process disclosed, or represents that its use would not infringe privately owned rights. Reference herein to any specific commercial product, process, or service by trade name, trademark, manufacturer, or otherwise, does not necessarily constitute or imply its endorsement, recommendation, or favoring by the United States Government or any agency thereof. The views and opinions of authors expressed herein do not necessarily state or reflect those of the United States Government or any agency thereof.

**PASSIVE DETECTORS**  
**Course on Advances in Radiation, International School of**  
**Radiation Damage and Protection Ettore Majorana Centre for**  
**Scientific Culture, Erice, Italy, September 1979**

Ralph H. Thomas

Lawrence Berkeley Laboratory  
 University of California  
 Berkeley, California

"They also serve who only stand and wait"

John Milton, 1608-1674  
 Sonnet XIX "On His Blindness"

**INTRODUCTION**

In this lecture I shall interpret the term "passive" radiation detector as meaning one that will yield up its information after an irradiation is completed, and often only after some processing of the detector to obtain the data or some considerable data processing. Examples of such detectors would thus be:

- (1) Nuclear Emulsion.
- (2) Activation Detectors (often imprecisely referred to as threshold detectors).
- (3) Integrating Ionization Chambers.
- (4) Thermoluminescent Dosimeters.

EB

## NUCLEAR EMULSIONS

The use of nuclear emulsion as a detector of ionizing radiations is, of course, as old as the discovery of radioactivity itself. Its use has persisted, particularly because nuclear emulsion provides a graphic presentation of nuclear interactions. It is partly for this reason that nuclear emulsions have played an extremely important role in the discovery of fundamental particles.<sup>1</sup> Whenever a new source of radiation is developed, almost inevitably one of the first exposures made is with some form of nuclear emulsion. As an example, Fig. 1 shows a microphotograph of the tracks of 2.1 GeV/amu nitrogen ions tracks in Ilford G5 emulsion. This emulsion was exposed shortly after heavy ions were accelerated at the Bevatron<sup>2,3</sup> and shows  $^{14}\text{N}_7$  ion fragmenting into two helium ions and three protons.

### Shielding Experiments

Thick nuclear emulsions were used in some of the earlier high-energy shielding experiments.<sup>4-6</sup> Figure 2 shows a microphotograph of a 10 GeV neutron in 600  $\mu$  Ilford G5 emulsion.<sup>7</sup> The use of emulsion facilitated studies of mean energy of the high energy particles as a function of depth in shielding, growth of the neutral component within the shield, angular divergence of

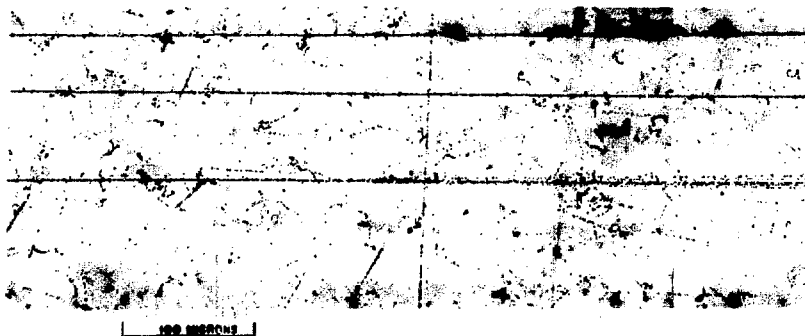


Figure 1. At a point on the left hand side of the figure an incident  $^{14}\text{N}_7^+$  ion fragments into two helium ions and three protons. The incident beam energy was 2.1 GeV/amu. and the nuclear emulsion was Ilford G5. (Courtesy of H. Heckmann).

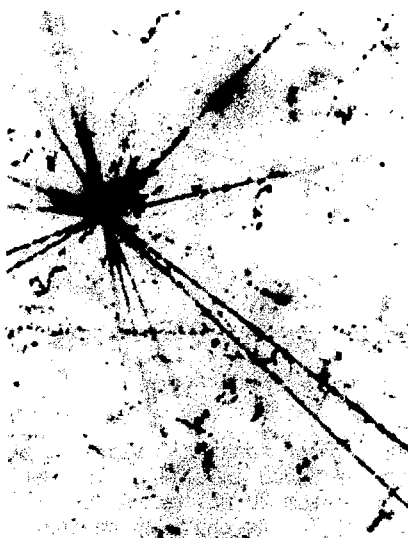
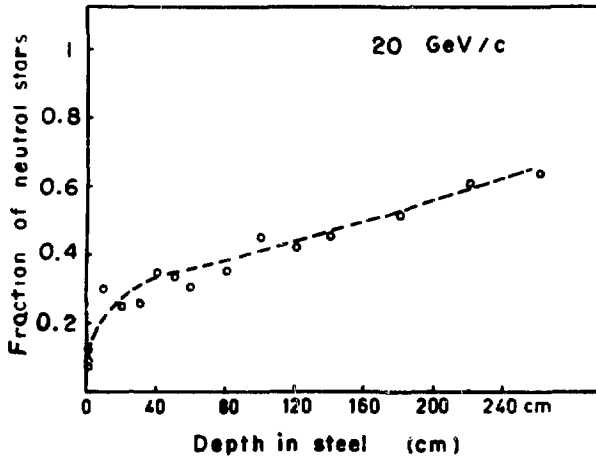


Figure 2. Photomicrograph of 10 GeV/c neutron interaction in Ilford G5 emulsion.

the beam, in addition to the overall attenuation of particle flux with depth. Thus, for example, Fig. 3 shows the fraction of "neutral" stars as a function of depth in steel irradiated with an incident 20 GeV/c proton beam.

#### Absolute Beam Intensity Measurements

Nuclear emulsions may be used for absolute beam intensity measurements. Smith et al.<sup>8</sup> have used Kodak NTA films to measure the intensity of carbon, oxygen, and neon ions. The films were exposed at an angle of  $45^\circ$  to the incident beam and the large ionization of the heavy ions produced dense tracks which are very easily identified (Fig. 4). Optimum exposures produce 40-20 tracks in a  $245 \mu\text{m}$  square field. The upper limit to track density that could be scanned with an air objective lens on the microscope (magnification 430x) was about  $4 \times 10^5$  tracks  $\text{cm}^{-1}$ . An oil immersion objective would raise this limit by about a factor of ten. This technique of beam intensity measurement was applied to the determination of radionuclide production cross sections,<sup>9</sup> measurement of the efficiency of



XBL7010-3948

Figure 3. The fraction of "neutral" stars as a function of depth in still. Incident proton momentum 20 GeV/c. A "neutral" star is defined as one with no charged primary in the backward hemisphere (after Citron et al.).

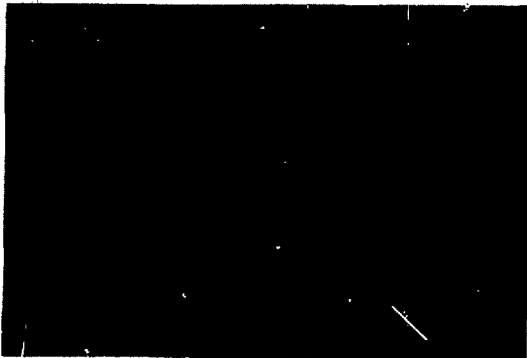


Figure 4. Photomicrograph of carbon ion tracks in Kodak NTA emulsion (magnification 430x).

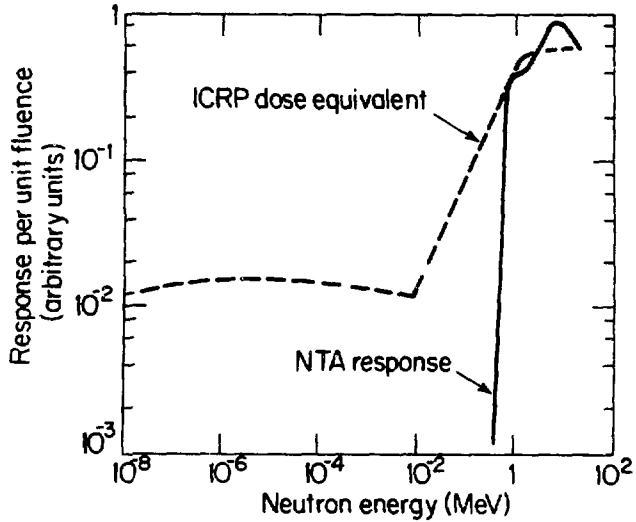
thermoluminescent dosimeters,<sup>10-12</sup> and to dosimetry in radiobiological experiments.<sup>13-15</sup>

### Personal Dosimetry

At the present time only three types of personal neutron dosimeters are commonly used in radiation protection.<sup>16</sup> The oldest and still most popular personal dosimeter is Kodak NTA film (or equivalent emulsions produced by other manufacturers), although in recent years it has become somewhat fashionable to denigrate the use of this dosimeter.<sup>17</sup> This criticism is based upon the inherent difficulties of the dosimeter, its instability, and its energy response. The dosimeter is read by detecting individual recoil proton tracks in a thin (25  $\mu\text{m}$ ) nuclear emulsion, using an optical microscope. While the technique seems laborious to those who prefer "gadgets," it is, nevertheless, in the hands of a skilled technician extremely reproducible, quite quick, and inexpensive.

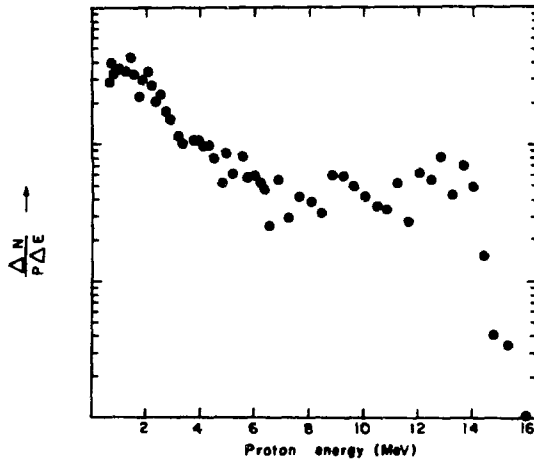
It has been known for many years that the latent image of the proton recoil tracks is unstable and fades, particularly at high temperature and humidities.<sup>18</sup> Much has been made of this fading<sup>19</sup> so that there has been a decline in the popularity of NTA film in recent years. This is, in the view of the writer, an error since it is certainly preferable to provide some personal dosimetry—rather than none of all! In fact the causes of latent image fading are well understood and it may be adequately controlled by careful packaging.<sup>20,21</sup>

The most serious disadvantage of NTA film is that it is limited to neutrons in the energy range from 0.5 MeV to about 20 MeV. Figure 5 shows the energy response of NTA film per unit neutron fluence, compared with the dose equivalent per unit fluence given by the ICRP. However, despite this limitation NTA film is of great value as a personal neutron dosimeter around high energy particle accelerators which the largest fraction of dose equivalent is due to neutrons from 0.5–20 MeV.<sup>23</sup> Some years ago the use of thick emulsions (200  $\mu\text{m}$ –600  $\mu\text{m}$ ) was proposed for neutron monitoring at high energies<sup>24,25</sup> but this suggestion has not been taken up.



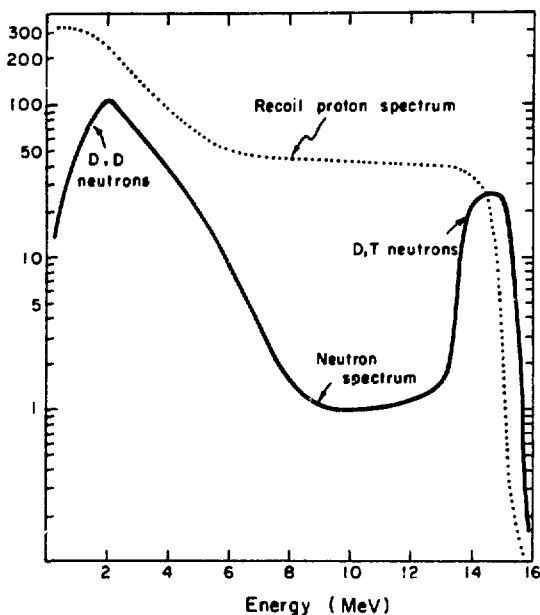
XBL 7910 4561

Figure 5. Energy response of NTA film.



XBL 787-3020

Figure 6a. Proton spectrum measured in an emulsion exposed to 14 MeV neutrons.



XBL729-4082

Figure 6b. Generation of a neutron spectrum from the proton recoil data shown in Figure 6a. The dotted line shows the smoothed curve fitted to the proton recoil scanning data, while the solid line shows the derived neutron spectrum.

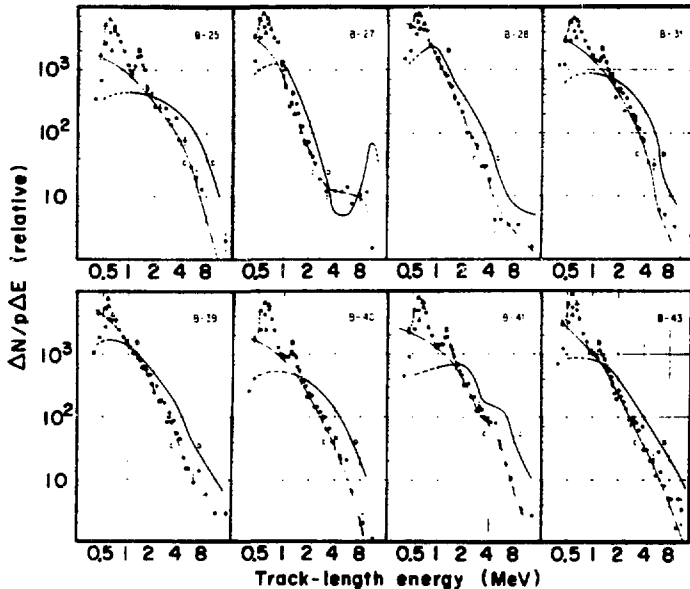
### Neutron Spectrometry

Nuclear emulsions have been used extensively for neutron spectroscopy and details of the techniques used may be found in Patterson and Thomas.<sup>26</sup> Two principal methods are used:

- (a) Proton recoil spectrum measurement
- (b) Star prong counting.

In the first technique the spectrum of recoil protons produced by neutron interactions in the emulsion is first measured, and then the neutron spectrum that produced it calculated. Figures 6a and 6b gives an example of the result obtained.

Figure 7 shows examples of neutron spectra measured by Lehmann and Fekula around the Bevatron.<sup>27</sup> The general form of the neutron spectra (measured between 0.7 and 20 MeV) at eight locations near the Bevatron is a broad peak in the 0.5-2 MeV region, followed by a smooth hundred-fold drop in value between the peak at 12 MeV.<sup>27</sup>



XBL729-1911

Figure 7. The neutron spectra derived from measurements of the recoil proton spectra in nuclear emulsions exposed at several locations around the Bevatron. In each diagram: A identifies the peak at 0.6 MeV due to the  $^{14}\text{N}(n,p)^{14}\text{C}$  reaction of thermal neutrons; B identifies the 1.25-MeV peak due to  $\alpha$ -particles from the decay of the naturally radioactive constituents of the emulsion; the curve C shows the smoothed recoil proton spectrum corrected for background, and the curve D shows the derived neutron spectrum. The notations B-25, B-27, etc., identify location of the emulsion exposure (after Lehman and Fekula, 1964).

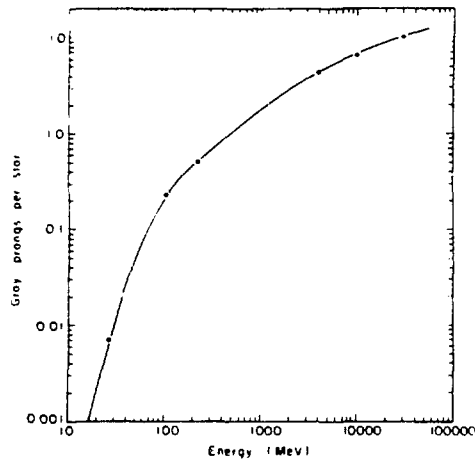


Figure 8. Average number of grey prongs per star as a function of neutron energy.

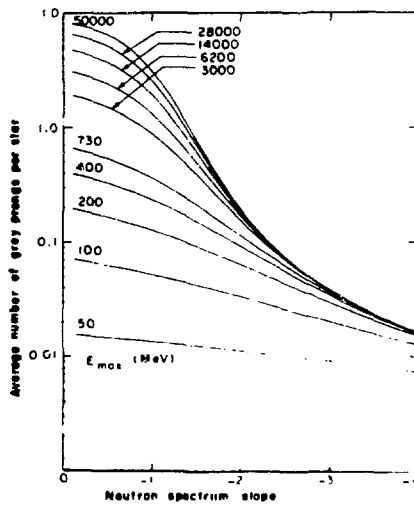


Figure 9. A graph relating the number of grey prongs per star and different shapes of neutron spectra characterized by the logarithmic slope,  $\gamma$ , and the maximum energy of the spectra.

Table 1. Spectral Indices Obtained from Measured Values of the Average Number of Gray Prongs per Star.

Location	$E_{\max}$ (MeV)	$\bar{n}_g$	Spectral index, $\gamma$
184-inch cyclotron between Bays 10 and 11	730	0.44	0.75
Bevatron west tangent tank shielding wall	6,200	0.55	1.50
Bevatron Col. 7, main floor	6,200	0.32	1.68
Bevatron mezzanine	6,200	0.27	1.78
CERN PS	14,000	0.29	1.80
CERN PS	14,000	0.21	1.95
CERN PS	28,000	0.45	1.68
White Mountain 12,000 ft. altitude	(50,000)	1.07	1.32
White Mountain 14,000 ft. altitude	(500,000)	1.04	1.35

The second application of emulsions to neutron spectroscopy is to determine the average number of gray prongs,  $\bar{n}_g$ , produced in the nuclear interactions. For monoenergetic neutrons there is a strong relationship between the average number of gray prongs per star and the incident neutron energy. This relationship has been determined by Remy<sup>28</sup> and by Patterson et al.<sup>29</sup> and is shown in Fig. 8. Patterson et al.<sup>29</sup> showed how to use this relationship to determine the characteristics of hard neutron spectra found around, for example, high energy accelerators. Under the assumptions that these spectra are smooth and may be characterized by an index,  $\gamma$ , that the cross section for star production is independent of neutron energy and that a maximum neutron energy may be defined, Patterson et al. calculated the relationship between  $\gamma$  and  $\bar{n}_g$  shown in Fig. 9, where several curves are shown for differing maximum energies. Thus, under the assumptions of the method, if  $\bar{n}_g$  is determined,  $E_{\max}$  known (e.g., as for example at an accelerator) then  $\gamma$  may be determined. Experience has shown that around accelerators  $\gamma$  has values usually in the range 1.3-20 (see Table 1).

Where independent checks have been possible—for example when spectra have been determined by alternative techniques, e.g., activation detectors—quite good agreement was obtained.<sup>30</sup> Patterson et al. concluded that "The study of stars in nuclear emulsion extends the usefulness of emulsion methods in nuclear spectroscopy to energies much higher than the upper limits of recoil proton techniques."<sup>29</sup>

\*The neutron differential energy spectrum  $d\phi/dE$  is written:  
 $d\phi/dE = E^{-\gamma}$ .

Table 2. Properties of Some Commonly Used Threshold Detectors.

Detector	Reaction	Half-Life	Energy range	Typical minimum flux density measurable <sup>a</sup> $n\text{ cm}^{-2}\text{s}^{-1}$	Remarks
BF <sub>3</sub> proportional counter	$^{10}\text{B}(n,\alpha)^7\text{Li}$	-	Thermal		
Gold foil	$^{197}\text{Au}(n,\gamma)^{198}\text{Au}$	2.7 days	Thermal	$10^2$	
Indium foil	$^{115}\text{In}(n,\gamma)^{116\text{m}}\text{In}$	54 min	Thermal	1	
Moderated BF <sub>3</sub> counter	$^{10}\text{B}(n,\alpha)^7\text{Li}$	-	Thermal-15 MeV	$10^{-2}$	Energy range and sensitivity depends upon moderator size -15 cm dia. values quoted.
Moderated gold foil	$^{197}\text{Au}(n,\alpha)^{198}\text{Au}$	2.7 days	Thermal-15 MeV	$10^2$	
Moderated indium foil	$^{115}\text{In}(n,\alpha)^{116\text{m}}\text{In}$	54 min	Thermal-15 MeV	1	
Thorium fission counter	Th(n,fiss.) fission products	-	>2 MeV	1	
Sulphur	$^{32}\text{S}(n,p)^{32}\text{P}$	14.3 days	>2.5 MeV	$10^4$	
Aluminum	$^{27}\text{Al}(n,\alpha)^{24}\text{Na}$	15 h	>6 MeV	1	
Aluminum	$^{27}\text{Al}(n,\text{spall.})^7\text{Be}$	53.4 days	>25 MeV	$10^4$	
Polystyrene: plastic scintillator	$^{12}\text{C}(n,2n)^{11}\text{C}$	20.4 min	>20 MeV	1	
	$^{12}\text{C}(n,\text{spall.})^7\text{Be}$	53.4 days	>30 MeV	$10^4$	
Bismuth fission chamber	Bi(n,f) fission products	-	>50 MeV	1	
Mercury	Hg(n,spall.) $^{149}\text{Tl}$	4.1 h	>600 MeV	10	

<sup>a</sup>Based on 1 h measurement.

## ACTIVATION DETECTORS

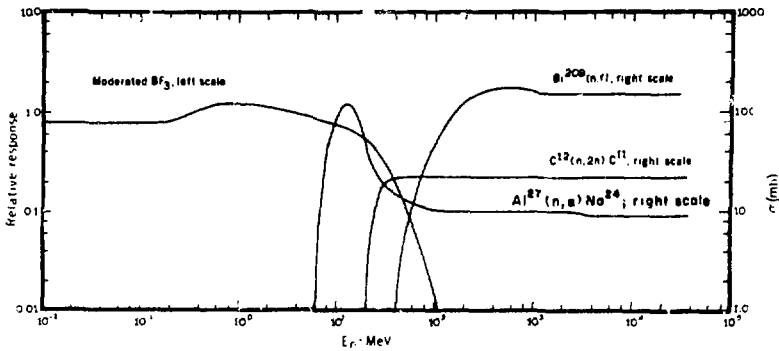
The use of threshold detectors in neutron dosimetry is a well understood and universally accepted technique in radiation physics. Their use has found widespread application at most high-energy particle accelerators and has been described in several articles, reviews and text books.<sup>23,26,30-34</sup>

Threshold detectors may be both active<sup>35</sup> and passive and both types of detector are frequently used in tandem in radiation surveys or other measurements.<sup>36</sup> We are particularly concerned here with threshold detectors that utilize their own induced radioactivity to monitor radiation.

Table 2 summarizes some of the threshold reactions commonly used as accelerator laboratories. Column 5 indicates the typical sensitivity which may be readily achieved for these detectors. Sensitivity is, however, clearly a function of detector size and the precise experimental techniques employed, and the values indicated are intended only as a general guideline. They indicate the order of magnitude of minimum flux density that may be detected after a measurement lasting one hour. For precise details, the reader is referred to the original sources. Furthermore, Table 2 is not intended to be comprehensive but to indicate the reactions in common use. Particular laboratories may have their own preferred specialties that they have perfected.

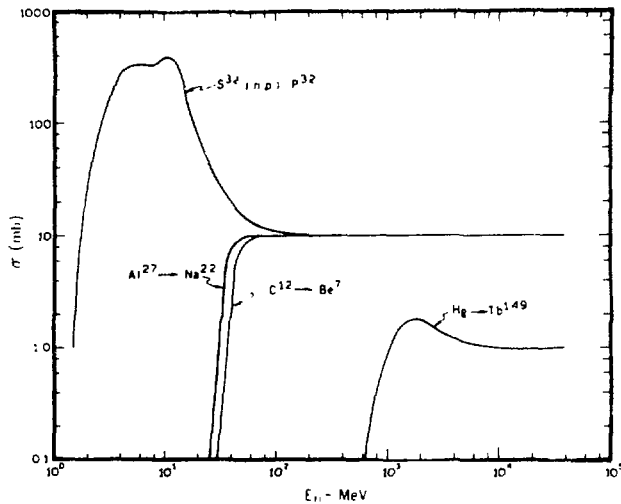
It may be seen from Table 2 that threshold detectors are of high sensitivity available over the entire energy range normally of interest at accelerators (0.1-100 MeV). No details of the shape of the neutron spectrum below about 1 MeV will be obtained using only one size of moderator with a thermal neutron detector. Fortunately such detail is not often required for two reasons: (1) because the dose-equivalent contribution is not large, and (2) because, below 10 keV, the dose-equivalent per unit fluence is independent of neutron energy. In principle, should more detailed information of the spectrum be required in the energy region from  $10^{-8}$  to 1 MeV, several moderators of different size could be used.<sup>37</sup>

At high radiation intensities ( $>10$  rem/h) several less sensitive reactions provide additional information. Figures 10a and 10b show the variation of sensitivity with energy for the reactions listed in Table 2.<sup>23</sup>



XBL 662 449:

Figure 10a. Response functions of four threshold detectors used to determine neutron spectra in well-shielded locations at high-energy accelerators. (After Thomas Ref. 23).



XBL 662 4492

Figure 10b. Response functions for additional detectors used to determine neutron spectra in high radiation levels at high-energy accelerators. (After Thomas Ref. 23).

Activation detectors are widely used radiation measurements at accelerators. Typical uses include:

- (a) Shielding Experiments
- (b) Neutron Spectrum Measurements
- (c) Radiation Surveys

### Shielding Studies

A great many shielding studies at high energy accelerators have been made using activation detectors. Many of these

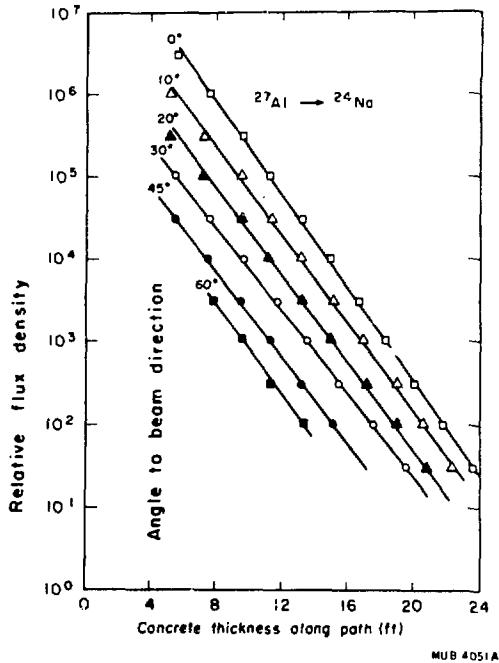


Figure 11. Relative flux density distribution measurements along paths drawn at several angles to the line of incidence of the proton beam, from the point of entry on a concrete shield. Measurements made with the  $^{27}\text{Al} \rightarrow ^{24}\text{Na}$  reaction. Incident proton energy 6 GeV. (After Smith et al. Ref. 34.)

measurements have been reviewed by Patterson and Thomas.<sup>38</sup> Figures 11 and 12 show typical examples of the data that may be obtained. Figure 11 shows the relative flux density distributions measured in a concrete shield bombarded by 6 GeV protons. The reaction used was the production of  $^{24}\text{Na}$  from  $^{27}\text{Al}$  (6 MeV threshold).

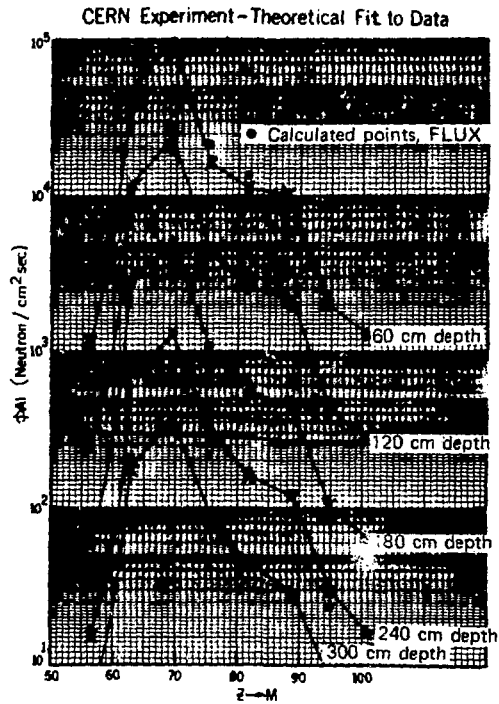


Figure 12. Measurements of neutron flux density in the earth shield of the CERN 28 GeV proton synchrotron. The crosses show experimental data points measured with the  $^{27}\text{Al} \rightarrow ^{24}\text{Na}$  reaction while the circles show calculated values. (Gilbert et al. Ref. 30).

Figure 12 shows experimental data using the same reaction obtained in the earth shield of the 28 GeV CERN Proton Synchrotron. The neutron flux density measured is plotted as a function of distance from the proton beam (depth) and along the beam direction (z). Measured values are in excellent agreement with those calculated using a computer program FLUXFT.<sup>30</sup>

To determine the spectrum a solution for the neutron spectrum  $\phi(E)$  is sought from a set of activation equations of the form

$$A_j = C_j \int_{E_{\min}}^{E_{\max}} \sigma_j(E) \phi(E) dE \quad \text{for } j = 1, 2, \dots, m \quad (1)$$

where

$A_j$  is the saturation activity of the  $j$ th detector,

$\sigma_j(E)$  is the cross-section for the appropriate reaction at energy  $E$ ,

$C_j$  is a normalizing constant between activity and flux density, and

$E_{\min}$ ,  $E_{\max}$  are the minimum and maximum neutron energies in the spectrum.<sup>30</sup>

Gilbert et al.<sup>30</sup> have described the use of an interactive technique that employs on-line facilities of a CDC-6600 computer for the determination of neutron spectra from a few threshold detectors: "TELLY." The operator indicates to the computer his best estimate of the neutron spectrum which will match his experimental data. This is done by drawing the spectrum with a light pen on the screen of a CRT display. The computer then calculates the detector responses and presents them for comparison with the experimental data. The operator then systematically modifies his suggested spectra to the computer until, after a few iterations, the detector responses are matched with an accuracy reflecting the experimental errors. TELLY was found to work well, avoiding many of the pitfalls of more "sophisticated" methods of spectrum analysis. Its only drawback is that it is somewhat difficult to use in a systematic manner when many detectors with overlapping regions of sensitivity are used.

Equation (1) is a degenerate case of a Fredholm integral of the first kind. Formal methods of solution are not applicable when, as is the case with activation detectors, the  $A_j$ 's are known only as a set of discrete points.<sup>39</sup>

Routti<sup>39</sup> has critically reviewed the numerical techniques commonly used for solution of such first-order Fredholm equations, and the interested reader is referred to his paper for a detailed account.

Early attempts to obtain neutron spectra from activation detector data were frustrated by difficulties such as non-uniqueness or an oscillatory (and even negative) character to the solutions to the Fredholm equations. Some of these problems arise from the mathematical characteristics of the equations to be solved, while others are related to the specific method of solution adopted.

Routti suggests that a suitable method of solution must be able to combine the information contained in the measured data with any already existing information of the neutron spectrum. Such prior information is almost always available on physical grounds. Thus, for example, the solution must be non-negative and zero beyond a given maximum energy. In addition, the spectrum of radiation penetrating thick shields constructed of a complex material such as concrete may be assumed to be smooth. Some information on intensity or shape may be available from previous measurements. It is important that all this prior information be properly taken into account in the solution technique selected. However, care must be taken to ensure that the consequent additional constraints imposed on the spectrum do not prevent it from matching the measured response or from assuming any physically acceptable shape.

Any appropriate solution must fulfill two basic measurements:

(a) The neutron spectrum which is found to be a solution to the activation equations must accurately match the detector responses; and

(b) if many solutions are found that fulfill condition (a), there should be a flexible way to apply physical prior information on the solution so that the most appropriate solution may be selected.

It is important that any solution method be tested to ensure that it meets all these requirements. This is most conveniently done by computing the response of the system to test spectra. The resolutions of the system and the influence of experimental errors or uncertainties in the detector response functions may then be systematically studied.

Routti has applied a generalized least-squares method to solve the activation equations. In his technique, the solution is forced to be non-negative and prior information on the

spectrum can be incorporated in a very flexible way. The technique and the computer program LOUHI, written to perform the analysis, have been subjected to the tests described in the previous paragraph. These tests show that the method meets the two basic requirements for an appropriate solution.

Considerable experience has now been obtained with LOUHI which has been found extremely reliable and capable of calculating neutron spectra with adequate accuracy for radiation protection purposes. A desirable feature of LOUHI is that, in addition to providing activation detector data, it may be used to determine neutron spectra from Bonner sphere or nuclear emulsion data.

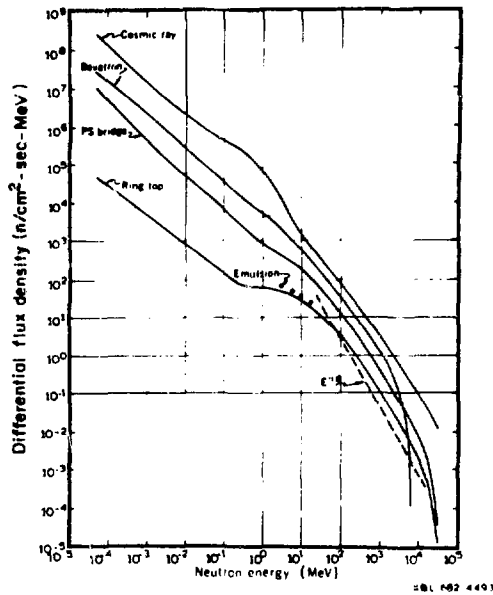
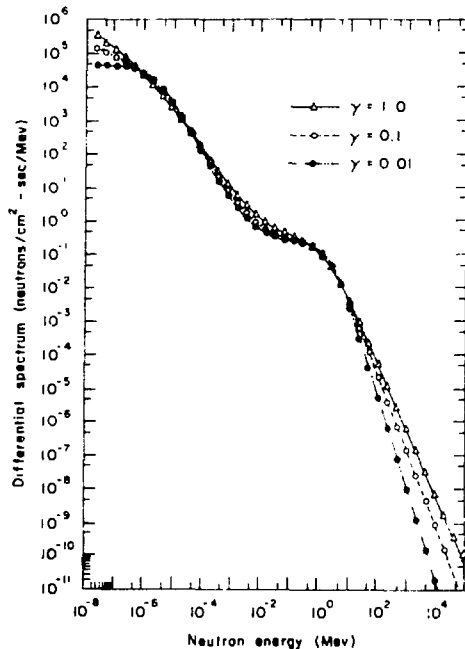


Figure 13. Typical high energy accelerator neutron spectra. The spectra are arbitrarily displaced on the vertical scale to show the differences between the spectra. The measurements shown here were made at the Bevatron and the CERN 28-GeV Proton Synchrotron - above concrete ("Bridge") and earth ("Ring Top"). In the case of the ring, top measurements were made with activation detectors (solid line), Ilford L4 emulsion (dots), and by star prong counting (dashed lines). The Hess cosmic ray spectrum is shown for comparison.

It is of interest to compare neutron spectra obtained using threshold detectors with those obtained from nuclear emulsions. This was possible in an experiment carried out at CERN where neutron spectra outside the shielding of the 28 GeV CERN proton synchrotron were determined by several methods.<sup>30</sup> Figure 13 shows several neutron differential energy spectra measured outside accelerator shields. In the case of one (labelled "Ring Top"), which was measured above the earth shield of the CPS neutron spectrum measurements, were made with activation detectors, proton recoil spectrum and gray prong number. The three spectra obtained are shown in the figure and are in reasonable agreement.



KB: 7711-108854

Fig. 14. Neutron differential energy spectra unfolded from data obtained in an aircraft flying at 41,000 ft, geomagnetic latitude 20°N, for various values of the smoothing parameter  $\gamma$ . (Stephens et al. Ref. 40).

Stephens et al.<sup>40</sup> have investigated the uncertainties in spectra unfolded by the LOUHI routine for the particular case of Bonner Spectrometer data. The LOUHI unfolding routine permits varying constraints to be placed on the rapidity and magnitude of fluctuations in the solutions it generates. This is achieved by the use of a smoothing parameter,  $\gamma$ , which normally is given values between 0 and 1.0. The higher value of  $\gamma$ , the more constrained are fluctuations in the solution generated and the lower the ability to resolve sharp structure in the spectrum. Figure 14 shows solutions for values of  $\gamma = 0.1$  (moderately damped) and  $\gamma = 0.01$  (slightly damped). Significant differences

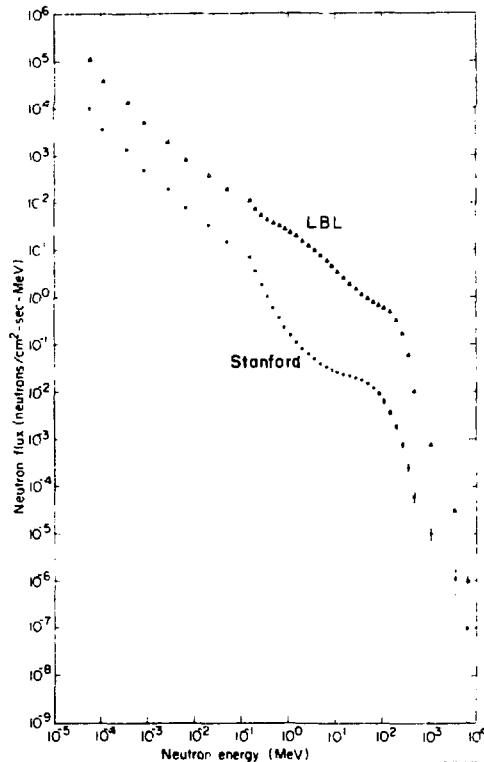


Fig. 15. Differential Neutron Energy Spectra measured at the Bevatron (LBL) and the Stanford 20 GeV electron linear accelerator (McCaslin et al. Ref. 41).

in the calculated spectra are evident, but it is not entirely clear whether this inconsistency is due to fluctuations of statistical origin or systematic errors introduced by the use of two detectors of different size and a mixed set of moderators. However, these authors also showed that the addition of data taken with aluminum activation detectors significantly limit the uncertainty in derived neutron spectra.

For some years there had been some difference in opinion between accelerator health physicists as to whether there was any significant dose equivalent contribution from neutrons with energy greater than 20 MeV. Activation detectors were applied to this problem.<sup>41</sup> Figure 15 shows the neutron differential energy spectra measured outside shielding at the 6 GeV proton synchrotron at Berkeley (the Bevatron) and the Stanford 20 GeV electron linear accelerator. From these spectra, the integral space dose equivalent curves may be calculated (Figs. 16 and 17). The integral dose equivalent spectra are quite similar and clearly show the presence of a significant high-energy neutron fluence at the Stanford Linear Accelerator, confirming theoretical predictions by de Staebler.<sup>42</sup>

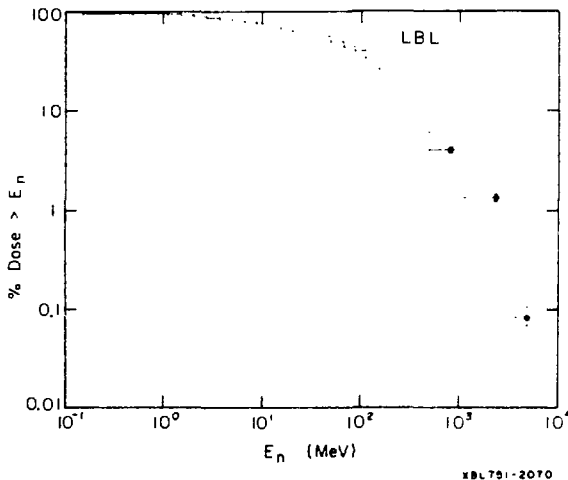


Figure 16. Integral dose equivalent spectrum (LBL).

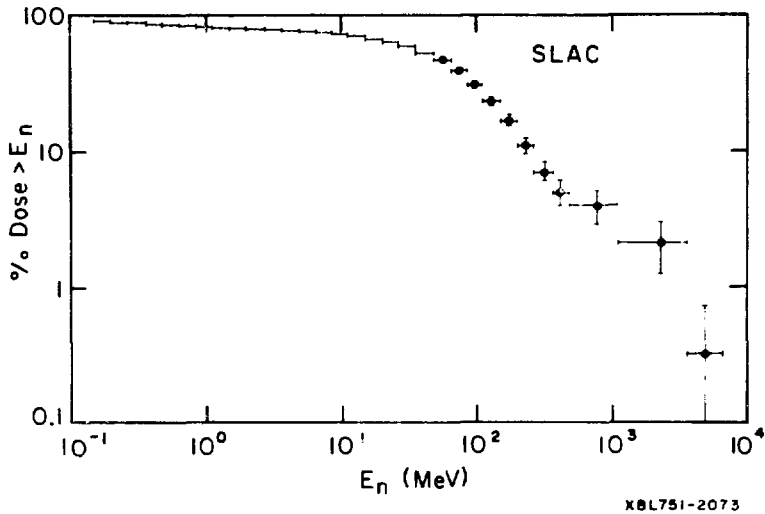
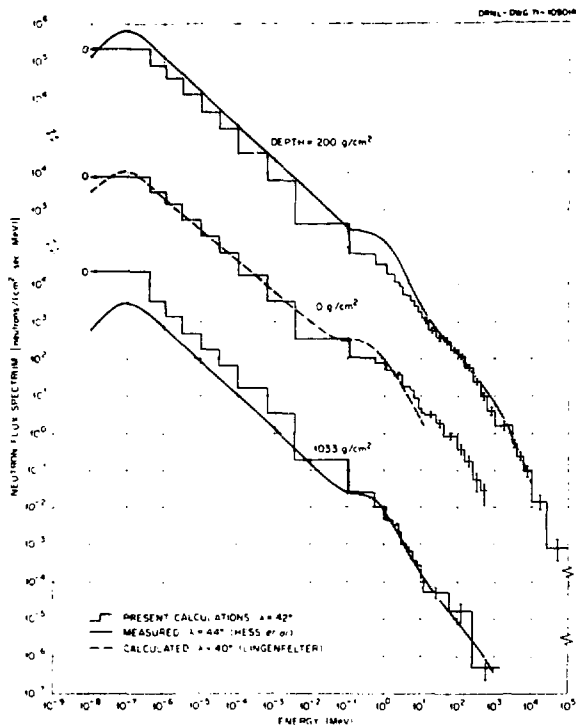


Figure 17. Integral dose equivalent spectrum (SLAC).

Despite the difficulties in measuring neutron spectra with threshold detectors the method may be used with some confidence as evidenced by the reasonable agreement between the experimental measurements of the cosmic-ray neutron spectrum by Hess et al.<sup>43</sup> made in 1958 and the relatively recent calculated values of Armstrong et al.<sup>44</sup> These workers used a Monte Carlo code to compute the production of protons, charged pions, and neutrons by the incident galactic protons, and the subsequent transport of these particles down to energies of 12 MeV. The calculated production of neutrons of energy  $\leq 12$  MeV calculated by the Monte Carlo code was used as input to a discrete-coordinates code to obtain the low-energy neutron spectrum. Figure 18 shows the results of these calculations and an absolute comparison with the experimental data of Hess et al.<sup>43</sup> at atmospheric depths of 200 and 1,033 g/cm<sup>2</sup>. The calculated and measured spectra differ somewhat at lower energies, but are in very good agreement at high energies.

#### The Use of Activation Detectors to Measure High-LET Radiation

Activation dosimeters have been used with great success in the absolute determination of particle fluences at proton



XBL 729-1939

Figure 18. Neutron flux spectra at various depths in the earth's atmosphere produced by galactic protons near solar minimum. These calculations are compared with calculations of Lingenfelter and the measurements of Hess et al. ( $\lambda$  = geomagnetic latitude) [Armstrong et al. Ref. 44].

accelerators and there is no reason to doubt that they might be used to monitor high-energy heavy-ion beam intensities.

The specific advantages of activation dosimeters are:

- (1) Suitable reactions give high activity enabling relative data of high statistical precision to be obtained. Such reactions may therefore be used as a standard with which the reproducibility and linearity of all other dosimetric systems may be compared.
- (2) The use of several activation detectors can give information on incident beam purity.

Smith<sup>45</sup> has reported initial tests of aluminum activation detectors irradiated by 375 MeV/u Ne<sup>10+</sup> ions. The induced <sup>24</sup>Na activity was measured using a NaI(Tl)  $\gamma$ -spectrometer situated in the Health Physics Department Low Background Facility.<sup>46</sup>

Sufficient activity is induced in 40 g of aluminum to easily obtain a statistical precision of  $\pm 1$  percent for exposures corresponding to 30 rad (the efficiency of the spectrometer used was  $\sim 35$  percent for <sup>24</sup>Na). Competing radionuclides produced were <sup>11</sup>C (20.3 min) and <sup>18</sup>F (110 min). The production of <sup>18</sup>F in aluminum is capable of comparable statistical precision to that obtained counting <sup>24</sup>Na, but correction for the production of <sup>11</sup>C (which also emits positrons) is an added complication.

Table 3 summarizes some possible activation reactions. As a general rule, those reactions that produce radionuclides with half-lives comparable to the length of irradiation will prove to be most convenient.

In radiobiological experiments it will often be convenient to use activation targets of composition similar to that in tissue, such as polyethylene, lucite, or polystyrene, in which the production of <sup>11</sup>C from <sup>12</sup>C is a convenient reaction. For absolute dosimetry, the reaction cross section must be known. Measurements for the production cross section of <sup>11</sup>C by 375 MeV/u Ne<sup>10+</sup> ions in carbon give a value  $75 \pm 7$  mb.<sup>9</sup> A reasonable compromise between energy loss in the target and sensitivity puts the lower limit of sensitivity for this reaction at an absorbed dose of  $\sim 10$  rad in tissue.

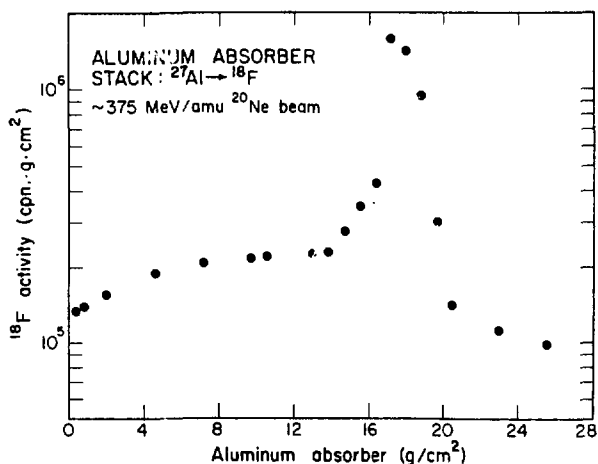
Activation detectors would be more acceptable in some experiments if they could be placed behind the irradiated biological sample to determine the particle fluence leaving the experiment, but it is then necessary to study the production of radionuclide to be measured as a function of depth in an

Table 3. Some Useful Target Activation Reactions that Produce Radionuclides with Half-lives Longer than about 10 Min.

Target material	Reactions useful for dosimetry			Competing and Reactions	
1. $^{27}\text{Al}$ in aluminum	$^{27}\text{Al} \rightarrow ^{24}\text{Na}$ $^{27}\text{Al} \rightarrow ^{22}\text{Na}$ $^{27}\text{Al} \rightarrow ^{18}\text{F}$ $^{27}\text{Al} \rightarrow ^{13}\text{N}$ $^{27}\text{Al} \rightarrow ^{11}\text{C}$ $^{27}\text{Al} \rightarrow ^7\text{Be}$	15.0 hr 2.60 yr 109.7 min 9.93 min 20.34 min 53.6 day	$\beta^-$ $e^-$ -capt, $\beta^+$ $\beta^+$ $\beta^+$ $\beta^+$ $e^-$ -capt	1368, 2754 keV 511, 1275 keV 511 keV 511 keV 511 keV 478 keV	
2. $^9\text{Be}$ in beryllium	$^9\text{Be} \rightarrow ^7\text{Be}$	53.6 day	half-life, $e^-$ -capt	478 keV	
3. $^{12}\text{C}$ in graphite, polystyrene, or polyethylene	$^{12}\text{C} \rightarrow ^{11}\text{C}$	20.34 min	$\beta^+$	511 keV	
4. $^{19}\text{F}$ in Teflon	$^{19}\text{F} \rightarrow ^{18}\text{F}$ $^{19}\text{F} \rightarrow ^{13}\text{N}$ $^{19}\text{F} \rightarrow ^{11}\text{C}$ $^{19}\text{F} \rightarrow ^7\text{Be}$	109.7 min 9.93 min 20.34 min 53.6 day	$\beta^+$ $\beta^+$ $\beta^+$ $e^-$ -capt	511 keV 511 keV 511 keV 478 keV	$^{12}\text{C} \rightarrow ^{11}\text{C}$ $^{12}\text{C} \rightarrow ^7\text{Be}$
5. $^{14}\text{N}$ in boron $^7\text{Be}$ nitride	$^{14}\text{N} \rightarrow ^{13}\text{N}$ $^{14}\text{N} \rightarrow ^{11}\text{C}$ $^{14}\text{N} \rightarrow ^7\text{Be}$	9.93 min 20.34 min 53.6 day	$\beta^+$ $\beta^+$ $e^-$ -capt	511 keV 511 keV 478 keV	$^{11}\text{B}, ^{10}\text{B}$
6. $^{16}\text{O}$ in water	$^{16}\text{O} \rightarrow ^{13}\text{N}$ $^{16}\text{O} \rightarrow ^{11}\text{C}$ $^{16}\text{O} \rightarrow ^7\text{Be}$	9.93 min 20.34 min 53.6 day	$\beta^+$ $\beta^+$ $e^-$ -capt	511 keV 511 keV 478 keV	
7. $^{16}\text{O}$ in beryllium oxide	$^{16}\text{O} \rightarrow ^{13}\text{N}$ $^{16}\text{O} \rightarrow ^{11}\text{C}$ $^{16}\text{O} \rightarrow ^7\text{Be}$	9.93 min 20.34 min 53.6 day	$\beta^+$ $\beta^+$ $e^-$ -capt	511 keV 511 keV 478 keV	$^9\text{Be} \rightarrow ^7\text{Be}$
8. $^{28}\text{Si}, ^{29}\text{Si}, ^{30}\text{Si}$ in fused quartz					

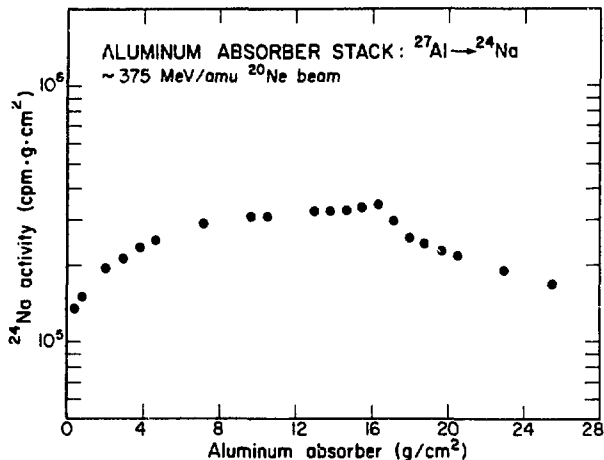
irradiated sample. Smith<sup>47</sup> has reported some preliminary studies of the distribution of  $^{18}\text{F}$  and  $^{24}\text{Na}$  in aluminum irradiated by 375 MeV/u  $\text{Ne}^{10+}$  ions. Figure 19 shows the distribution of  $^{18}\text{F}$  in aluminum. The initial portion of the  $^{18}\text{F}$  curve is caused by the production of  $^{18}\text{F}$  fragments from the original neon ion beam.<sup>48</sup> Such fragments have a range of  $\sim 17 \text{ g cm}^{-2}$  in aluminum and are thus seen superposed on the continuous distribution of  $^{18}\text{F}$  due to target activation. Beyond the range of the primary ions ( $\sim 16\text{--}17 \text{ g cm}^{-2}$ ),  $^{18}\text{F}$  is produced by the reaction of lighter fragments with the target aluminum (residual activation). The total  $^{18}\text{F}$  due to stopped fragments is approximately equal to that due to target activation. Residual activation is not insignificant being nearly of the same magnitude as that due to target activation at the entrance of the stack. The total quantity of residual  $^{18}\text{F}$  activity is, however, only a few percent of that due to target activation because it rapidly decreases with increasing depth, beyond the primary ion range.

The distribution of  $^{24}\text{Na}$  is shown in Fig. 20 and exhibits the typical buildup of activity as a function of depth observed in high-energy irradiations. Beyond the range of the primary ions there is a sharp reduction in  $^{24}\text{Na}$  production. Residual activation is seen to be higher beyond the neon ion range than the target activation at the target entrance. Since  $^{24}\text{Na}$  is



XBL 757-3418

Figure 19. The distribution of  $^{18}\text{F}$  along an aluminum target bombarded by 375 MeV/amu  $\text{Ne}^{10+}$  ions.



XBL 757-3417

Figure 20. The distribution of  $^{24}\text{Na}$  activity along an aluminum target bombarded by 375 MeV/amu  $\text{Ne}^{10+}$  ions.

heavier than the primary ions ( $^{20}\text{Ne}$ ), autoactivation is not feasible.

These preliminary studies indicate the need to study the three mechanisms of activation in some detail if activation techniques are to be used for absolute dosimetry behind considerable thickness of material. Smith<sup>49</sup> has reported approximate cross sections for the production of  $^{18}\text{F}$  and  $^{24}\text{Na}$  in several materials irradiated by 375 MeV/u  $\text{Ne}^{10+}$  ions. Table 4 summarizes these values.

Recently, work at Los Alamos has used the production of  $^{24}\text{Na}$  in  $^{27}\text{Al}$  for pion in-vivo dosimetry. They report that the  $^{24}\text{Na}$  activity is primarily produced by stopping  $\pi^-$  mesons, but that 15–25 percent of the activity results from neutrons. Comparison of the induced activity distributions with the high-LET absorbed dose measured by a silicon detector and a Rossi chamber show that the  $^{24}\text{Na}$  activity may be used as a good measure of the high-LET dose.<sup>50</sup>

#### IONIZATION CHAMBERS

The charge  $Q$ , collected under conditions of electronic equilibrium as a result of the passage of a number  $N$  of particles

Table 4.  $^{11}\text{C}$  Production Sections—375 MeV/u  $\text{Ne}^{+10}$  Ions.

Target	Reaction	Production cross-section (m barn)
Al	$^{24}\text{Na}$	63
Si	$^{24}\text{Na}$	15
S	$^{24}\text{Na}$	11
Al	$^{18}\text{F}$	40
Si	$^{18}\text{F}$	36
S	$^{18}\text{F}$	16

across the plates of a parallel-plate ionization chamber placed normally to a uniform, parallel charged particle beam, is related to the average energy required to create an ion pair,  $w$ , by the equation:

$$Q = \rho e \frac{N}{w} \Delta E \quad (2)$$

where  $w$  is measured in eV and

$\rho$  is the density of nitrogen in the ionization chamber,  $\text{g cm}^{-3}$ ;

$e$  is the electronic charge, coulomb;

$\Delta E$  is the energy absorbed in the gas, eV.

If the energy of the incident particles is high, the energy loss in passing through the gas is small and equation (2) may be written:

$$Q = 10^6 s e \left( \frac{dE}{dx} \right)_{\text{N}_2} \cdot \frac{N}{w} \quad (2a)$$

where  $s$  is the separation between the collection plates, cm;

$\left( \frac{dE}{dx} \right)_{\text{N}_2}$  is the mass stopping power of the particles in the nitrogen within the chamber,  $\text{MeV g}^{-1} \text{cm}^2$ .

Equation (2a) may be related to the absorbed dose in tissue,  $D$ , by the equation:

$$D = 10^5 Q \frac{\bar{w}}{m} S' \quad (3)$$

where  $m$  is the mass of irradiated gas in the chamber (in grams)

$S'$  is the ratio of stopping powers of tissue to gas for the incident particles.

The Biology and Medicine Division of the Lawrence Berkeley Laboratory has designed large parallel-plate, nitrogen-filled ionization chambers for dosimetry in radiobiological experiments. These chambers are constructed so as to present a minimum of absorbing material ( $\sim 0.05 \text{ g cm}^{-2}$ ) in the heavy ion beam

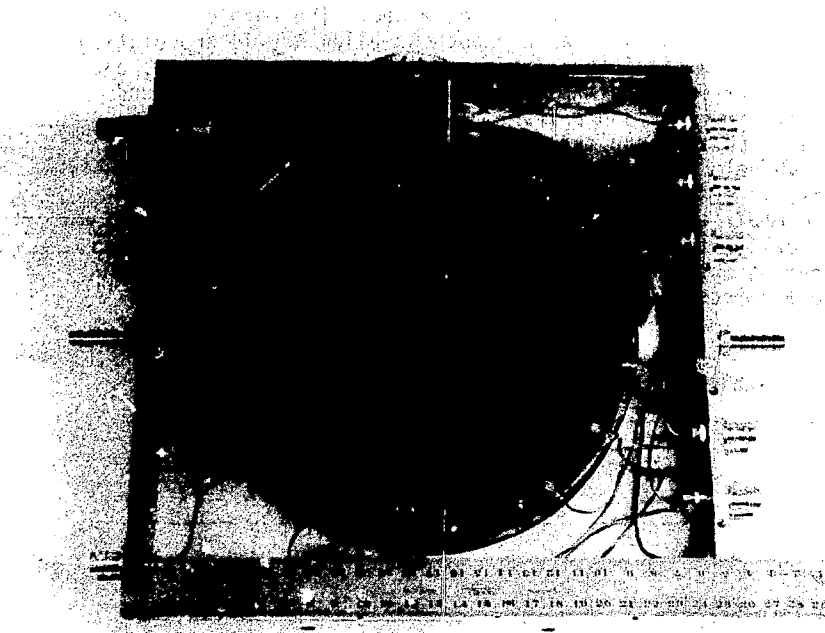


Figure 21. Photograph of a prototype annular ionization chamber used for Biomedical dosimetry.

path. The electronic equilibrium established in the air path through which the beam passes before entering the chamber is essentially maintained as the beam passes through the chamber. The collecting electrodes of the chambers are circular in cross section, and are spaced 1 cm from the high voltage electrode and placed at right angles to the incident beam direction.

Many radiobiological experiments at the Bevalac utilize rather large irradiation fields (typical beam dimensions might in some cases be a fullwidth, half maximum of 10-12 cm). Chambers have been constructed with collecting electrodes up to 18 cm in diameter to make measurements in such radiation fields. Each collecting electrode is divided into several regions which make it possible to use the chambers to explore the uniformity of the radiation fields used in the experiments (Fig. 21).

For accurate dosimetry, values of  $\bar{w}$  must therefore be known. There were until recently no values of  $\bar{w}$  published in the literature for high energy ions (a few hundred MeV/amu). Thomas and his colleagues have reviewed the literature and described measurements of  $\bar{w}$  for 250 MeV/amu  $^{12}\text{C}^{6+}$  ions, 375 MeV/amu  $^{20}\text{Ne}^{10+}$  ions and 479 MeV/amu  $^{40}\text{Ar}^{18+}$  ions.<sup>51,52</sup>

Table 5 summarizes the values obtained. The absolute errors are  $\pm 5$  percent and just large enough to allow the interpretation that there is no significant difference between one another, and even that they do not differ from the value used for electrons  $w_B$ , of  $34.6 \pm 0.3$  eV/ion pair.<sup>53</sup> If this interpretation of the data is chosen then the suggestion by Bakker and Segre that  $\bar{w}$  for high velocity particles would tend to the value  $w_B$  (Ref. 54) is confirmed. This suggestion was, however, based upon the empirical evidence available at that time (1961). Theoretically, there are grounds for expecting the value of  $\bar{w}$  to be dependent upon LET. As the LET of the ion increases, there will be a correspondingly greater energy density around the

Table 5. Values of  $w$  for Heavy Ions.

Ion Species	Energy (MeV/amu)	$w$ (eV)
$^{12}\text{C}^{6+}$	250	$36.3 \pm 1.9$
$^{20}\text{Ne}^{10+}$	375	$35.3 \pm 1.5$
$^{40}\text{Ar}^{18+}$	479	$34.6 \pm 0.9$

particle trajectory, which in turn increases the probability of ionic recombination, leading to higher values of  $\bar{w}$ . However, comparison of the published values of  $\bar{w}$  shows this variation is probably not larger than about 10-15 percent.<sup>55,56</sup>

The data of Thomas et al.<sup>52</sup> do indeed show a trend of decreasing  $\bar{w}$  with increasing charge state of the ion and increasing energy. Their accuracy, however, does not permit definitive conclusions and additional and more accurate measurements are needed.

The values of  $\bar{w}$  obtained thus far give estimates of absorbed dose in tissue which are in good agreement with values obtained by other experimental techniques. Thus, Patrick et al.<sup>13</sup> have compared measurements of the entrance absorbed dose in soft tissue irradiated by 250 MeV/amu  $C^{6+}$  ions using a nitrogen filled ionization chamber and  $^7LiF$  thermoluminescent dosimeters. Table 6 summarizes the results. The error for the ionization chamber measurements were  $\pm 5$  percent. Only statistical errors are included for the TLD measurements in the table. The absolute uncertainty was about  $\pm 3$  percent. The two sets of absorbed dose estimates are seen to be in good agreement.

Table 6. Comparison of Entrance Absorbed Dose in Issue Irradiated by 250 MeV/u Ions

Irradiation No.	Group No.	Entrance Absorbed Dose in Tissue		Ratio ionization chamber to TLD
		(red.) Ionization chamber <sup>a</sup>	(LiF) Thermoluminescent dosimeter <sup>b</sup>	
1	a	64.0 $\pm$ 3.2	61.2 $\pm$ 0.5	1.045
1	b	96.6 $\pm$ 4.8	93.6 $\pm$ 0.9	1.032
2	a	128 $\pm$ 6.4	124 $\pm$ 2	1.032
2	b	193 $\pm$ 10	186 $\pm$ 4	1.038

<sup>a</sup>Using a value  $W = 36.6$  eV/ion pair. Errors  $\pm 5$  percent.

<sup>b</sup>Using a value  $e = 0.89$ . Statistical errors only.

Table 7. Characteristics of TL Phosphors.

Characteristic	LiF	Li <sub>2</sub> B <sub>4</sub> O <sub>7</sub> :Mn	CaF <sub>2</sub> :Mn	CaF <sub>2</sub> :nat	CaSO <sub>4</sub> :Mn
Density (gm/cc)	2.64	2.3	3.18	3.18	2.61
Effective atomic no.	8.2	7.4	16.3	16.3	18.3
TL emission spectra(Å) range maximum	3500-6000 4000	5300-6300 6050	4400-6000 5000	3500-5000 3800	4500-6000 5000
Temperature of main TL glow peak	195°C	200°C	260°C	260°C	110°C
Efficiency at Cobalt-60 (relative to LiF)	1.0	0.3	3	23	70
Energy response without added filter (30 keV/Cobalt-60)	~1.25	0.9	13	13	10
Useful range	mR-10 <sup>5</sup> R	mR-10 <sup>5</sup> R	mR-3 x 10 <sup>5</sup> R	mR-10 <sup>4</sup> R	R-10 <sup>4</sup> R
Fading	small, 5 /12 wk	10 in first month	10 in first month	no detectable fading	50 -60 in the first 24 hrs
Light sensitivity	essentially none	essentially non	essentially none	yes	yes
Physical form	powder, extruded, Teflon-embedded, silicon-embedded, glass capillaries	powder, Teflon- embedded	powder, Teflon- embedded, hot- pressed chips, glass capillaries	special dosimeters	powder, Teflon- embedded

## THERMOLUMINESCENT DOSIMETERS

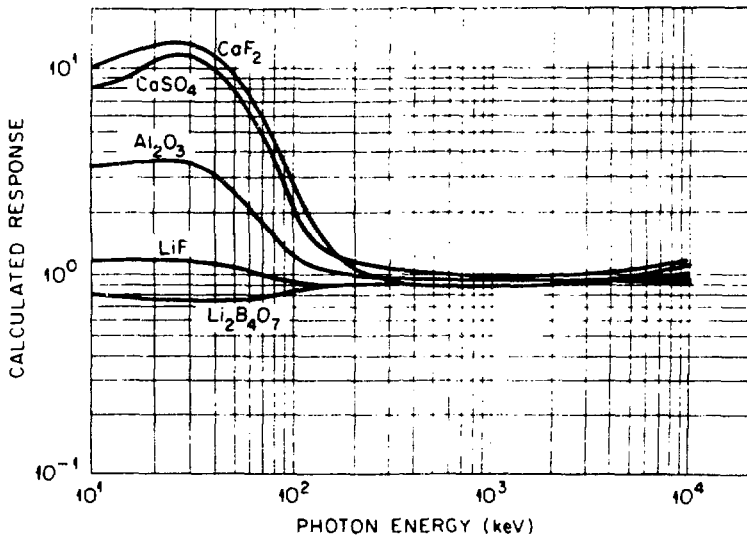
Thermoluminescent dosimeters are now widely used as personal dosimeters,<sup>57</sup> for measurements of environmental radiation<sup>58</sup> and in radiological physics.<sup>59</sup>

The basic technique has been known for more than three hundred years and was first used to measure ionizing radiation by Weidmann and Schmidt in 1895.<sup>60</sup>

In the past twenty years several phosphors have been developed but easily the most widely used is Lithium fluoride. Table 7 shows the characteristics of several thermoluminescent phosphors and Fig. 22 shows that relative response of several phosphors as a function of photon energy.

### Lithium Fluoride Phosphors

It is the rather flat energy response of LiF that has made it so popular for photon dosimetry (the difference in response between 40 keV and 1 MeV is only 30 percent). However, LiF phosphors present



XBL 7912-13627

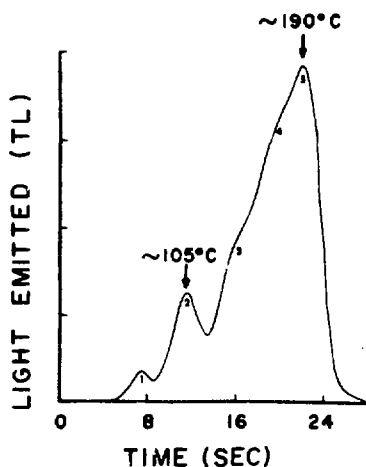
Figure 22. Theoretical sensitivity of several thermoluminescent phosphors.

some difficulties, demanding very careful technique if they are to be used for accurate dosimetry.

The glow curve is complex and far from ideal, as may be seen from Fig. 23 which shows a typical glow curve after the phosphor has been annealed at 1 hr at 400°C, irradiated to 100 R, and then immediately read.

The glow curve is complex showing 5 peaks. These peaks decay at room temperature with approximate half-lives of 5 minutes, 10 hours, 0.5 years, 7 years, and 80 years. Peaks 4 and 5 are the most suitable for dosimetry. Peaks 1 and 2 may be removed by various combinations of pre- and post-irradiation annealing. Post-irradiation annealing for 10 minutes at 100° is usual.

Annealing procedures can have a significant influence on the sensitivity of LiF phosphors and carefully controlled technique is required for consistency.<sup>59</sup> The light output from LiF phosphors is linear up to an exposure of about 1000 R as may be seen in Fig. 24 and the output is photon dose-rate independent up to dose rates of at least  $2 \times 10^{11}$  rads  $s^{-1}$ . LiF in its pure form exhibits little thermoluminescence, the phenomenon depending



NBL 748-1376

Figure 23. Typical glow curve of LiF (TLD-100) after phosphor has been annealed 1 hour at 400°C read soon after irradiation to 100 R.

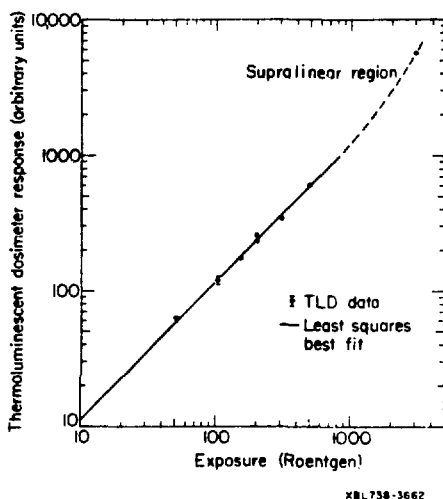


Figure 24.  ${}^7\text{LiF}$  thermoluminescent dosimeter response to  $60\text{r}_0$   $\gamma$ -rays. One representative error bar is indicated.

upon the correct mix of impurity ingredients. There is no general agreement as to what these are but Mg, Eu, Y, Zr, and Ce have been reorted in various descriptions of techniques of production. (Harshaw manufactures LiF: Mg, Ti under the trade-names TLD-100, 600 and 700, and the composition of these phosphors is shown in the Table 8.)

The main dosimetry peak is around  $200^\circ$  which is favorable for rapid heating. the emission spectrum from LiF lies in the

Table 8. Isotopic Composition of Some LiF Phosphorus.

Isotope	TLD-100	TLD-600	TLD-700
${}^6\text{Li}$	7.5	95.6	0.01
${}^7\text{Li}$	92.5	4.4	99.99

blue region enabling infra-red emission from the heater to be eliminated by the use of a red/infra-red filter.

### Neutron Detection

The high thermal neutron capture cross section of  ${}^6\text{Li}$  has led to the use of  ${}^6\text{LiF}$  phosphors for neutron detection both in personal dosimetry and to measure fast neutrons by surrounding them with moderator—as for example, Bonner spheres.<sup>62</sup> Since TLD 600 contains 95.6 percent  ${}^6\text{Li}^+$ , TLD 700 99.99 percent  ${}^7\text{LiF}$ , a pair of dosimeters can be used to measure thermal neutron exposures by difference.

Cameron et al.<sup>60</sup> found that TLD-100 gives the following light output:

$$10^9 \text{ neutrons cm}^{-2} (\sim 1 \text{ rem}) \cong 37\text{R } {}^{137}\text{Cs } \gamma\text{-rays} \quad .$$

On the basis of energy absorbed thermal neutrons produce  $\sim 1/7$  the amount of light produced by  $\gamma$ -rays.

Because of the high thermal neutron capture cross section of  ${}^6\text{Li}$  some care must be taken in measurements using  $\text{LiF}$  phosphors when neutrons are present. It should be noted that:

- (a) Traces of  ${}^6\text{Li}$  in TLD-700 may give errors.
- (b) TLD-100 and TLD-600 have large capture cross sections for thermal neutrons. Samples must therefore be thin: (~0.1 mm of TLD-100 absorbs 5-10 percent incident thermal neutrons. ~0.1 mm of TLD-600 absorbs 50 percent of incident thermal neutrons.)
- (c) Fast neutrons may be moderated by the human body to produce thermal neutrons.
- (d) The glow curves for photons and thermal neutrons are slightly different.
- (e) Supralinearity is less for thermal neutrons than for photons.

### Response of $\text{LiF}$ Phosphors to Charged Particles

$\text{LiF}$  phosphors are sensitive to electrons, protons, alpha particles and heavy ions. In general the light output per unit

of energy absorbed decreases with the LET of the incident radiation.

Jahnert<sup>60</sup> has reported measurement of the efficiency of the light output of TLD-700 ( ${}^7\text{LiF}$ ) using protons from a few to 20 MeV and alpha-particles emitted by radioactive materials. He found decreasing efficiency with increasing LET.

Jahnert has proposed two alternative theoretical models (which differ in the number of electron traps assumed), both of which fit his experimental data quite well in the range of LET from 0.02 to 300 keV/m, when the accuracy of the experimental data is considered. The one-trap theory seems to fit the data better and may be used to interpolate values of  $\epsilon$ . Jahnert's work has been continued using energetic heavy ions by Thomas and his colleagues.<sup>10-12</sup>

The Bevalac is capable of producing heavy ions as heavy as  $\text{Ar}^{+18}$ , up to energies as high as 2.1 GeV/amu.<sup>61</sup>  ${}^7\text{LiF}$  dosimeters were exposed to carbon, oxygen, neon and argon ions of energies shown in Table 9. The experimental technique used was to expose the dosimeter simultaneously with nuclear emulsions (Kodak type NTA), AgCl crystal detectors<sup>62</sup> or activation detectors to determine the particle fluence,  $\phi$ . The absorbed dose in the irradiated dosimeters may then be calculated from their known stopping power,  $(dE/dx)_{\text{LiF}}$ , for the incident ions. Finally, the dosimeter response to heavy ions,  $L$ , is compared with the dosimeter response to  ${}^{60}\text{Co}$  photons for an exposure of 1 R,  $\tau$ .

Table 9. Measurements of  $\epsilon$ .

Ion Species	Energy (MeV/amu)	$(dE/dx)$ in ${}^7\text{LiF}$ (MeV $\text{g}^{-1}\text{cm}^2$ )	
$\text{H}^{+1}$	798	1.89	$1.08 \pm 0.08$
$\text{C}^{+6}$	252	116	$0.89 \pm 0.02$
$\text{O}^{+8}$	300	112	$0.90 \pm 0.05$
$\text{O}^{+8}$	1050	186	$0.82 \pm 0.05$
$\text{Ne}^{+10}$	372	259	$0.73 \pm 0.03$
$\text{A}^{+18}$	447	770	$0.52 \pm 0.02$

It may then be readily shown that

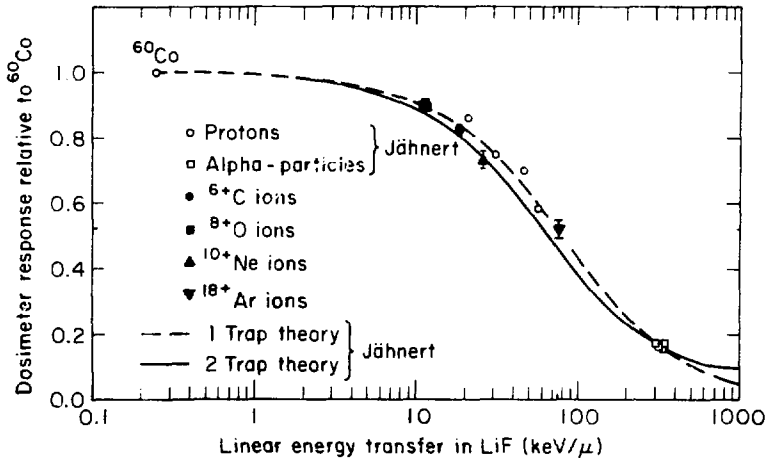
$$\epsilon = \frac{5.05 \times 10^7}{\left(\frac{dE}{dx}\right)_{\text{LiF}}} \cdot \frac{L}{\phi} \quad (4)$$

when  $L$  and  $\tau$  are light outputs in arbitrary units, and

$$\left(\frac{dE}{dx}\right)_{\text{LiF}} \text{ is measured in MeV g}^{-1} \text{ cm}^{-2},$$

$$\phi \text{ is measured in particles cm}^{-2}.$$

Figure 25 summarizes the data of Jähner<sup>63</sup> and Thomas et al.,<sup>10-12</sup> together with theoretical predictions.



XBL 754 - 2639

Figure 25. Measured values of  $^7\text{LiF}$  TLD efficiency relative to  $^{60}\text{Co}$   $\gamma$ -rays and comparison with theoretical models.

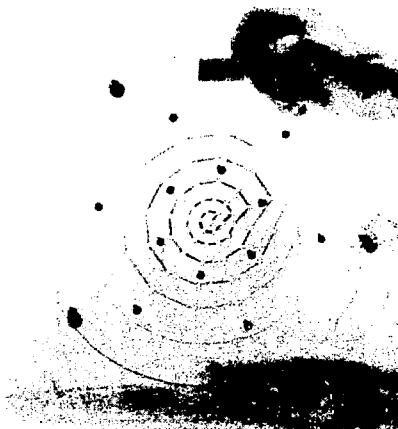


Figure 26. Lucite assembly used to determine spatial distribution of absorbed dose in heavy ion irradiation fields.

These studies have enabled  $^7\text{LiF}$  phosphors to be used for accurate heavy ion dosimetry (few percent) but more fundamental work remains to be done. The light output as a function of absorbed dose due to heavy ions can be inferred to be linear from a few rads to about 500 rads by the work of Thomas et al.,<sup>10-12</sup> but controlled experiments are needed. Dose rate phenomena need to be investigated and details of the glow curves as a function of ion species, absorbed dose and dose rate must be studied. Nevertheless LiF phosphors are extremely valuable tools having a wide range of application in particle dosimetry.

#### Measurement of the Spatial Variations of Radiation Fields

$^7\text{LiF}$  dosimeters are useful in field intensity mapping. Smith et al.<sup>8</sup> have reported measurements using 0.125 in. x 0.125 in. x 0.035 in. mass ~25 mg phosphors, manufactured by the Harshaw Chemical Company. Figure 26 shows a dosimeter assembly that may be placed in the radiation field, while Fig. 27 shows the spatial distribution of absorbed dose across a beam of 380 MeV/amu<sup>10+</sup> Ne ions.

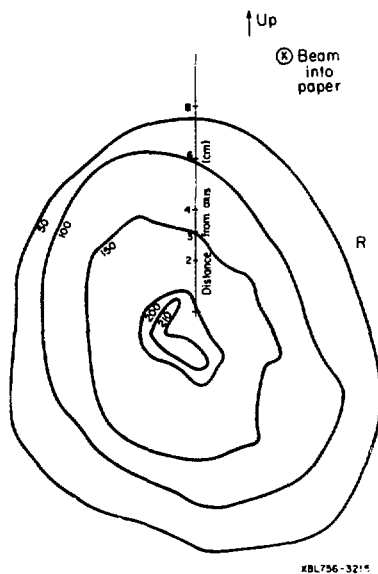
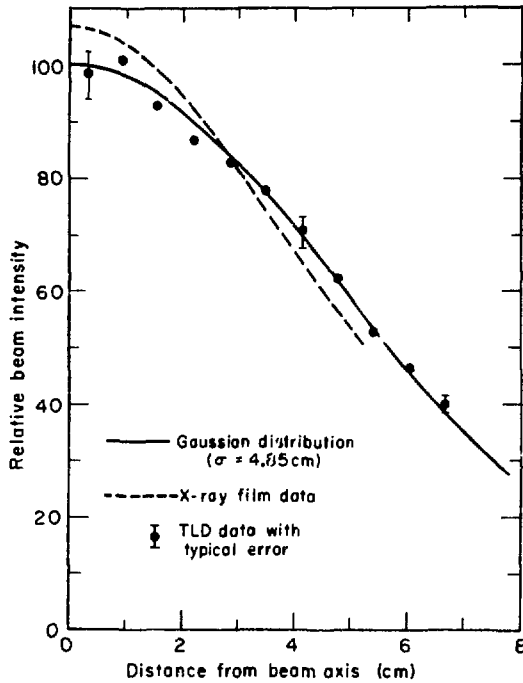


Figure 27. Spatial distribution of absorbed dose around a  $10^+$ Ne beam used to irradiate mice. Determined using  $^7\text{LiF}$  thermoluminescent dosimeters.

Patrick et al.<sup>13</sup> report reasonable agreement between beam profile measurements made using  $^7\text{LiF}$  dosimeters and Du Pont NDT-45 X-ray film, as may be seen by inspection of Fig. 28.

#### Absorbed Dose Distribution Studies

Thermoluminescent dosimeters are also extremely useful for absorbed dose distribution studies. Patrick et al.<sup>13</sup> have reported measurements of the spatial distribution of absorbed dose in a lucite cylinder (used to simulate irradiated mice) irradiated by a wide beam of 251 MeV/amu  $^{6+}\text{C}$  ions. Figure 29 shows both the dosimeter response and the calculated absorbed dose distribution using energy-loss data of Steward et al.<sup>63</sup>



XBL 737-9538

Figure 28. Comparison of a carbon ion beam profile measured with X-ray film and TLD.

Secondary particles resulting from primary particle interactions are not taken into account in the calculated curve. Comparison between the calculated curve and dosimeter readings is not precisely possible because the dosimeter efficiency is a function of LET and changes along the length of the phantom and these effects must be taken into account for precision. However, the general agreement between the two sets of data is gratifying.

#### ACKNOWLEDGEMENT

This work was supported by the U. S. Department of Energy under contract No. W07405-ENG-48.

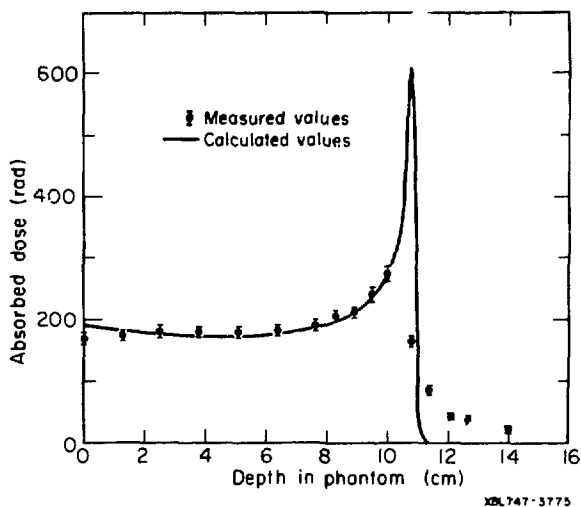


Figure 29.  ${}^7\text{LiF}$  Thermoluminescent Dosimeter response as a function of depth in a lucite phantom irradiated by a broad beam of 251 MeV/amu  ${}^6\text{C}^+$  ions. The measurements are compared with calculated values of the energy deposition from ionization energy losses.

#### REFERENCES

1. C. F. Powell, 1959, "The Study of Elementary Particles by the Photographic Method," Pergamon Press, Oxford.
2. R. H. Thomas, 1972, High Energy Heavy Ions, Phys Bull. 23: 143.
3. H. A. Grunder et al., 1971, Acceleration of Heavy Ions at the Bevatron Science, 174: 1128.
4. A. Citron, L. Hoffmann and C. Passow, 1961, Nucl. and Meth. 14: 97.
5. R. H. Thomas (ed.), 1963, Report of the Shielding Conference held at the Rutherford Laboratory, Sept. 26-27th, 1962, Rutherford Laboratory Report NIRL/R/40.
6. H. Bindewald et al., 1965, Shielding Studies in Steel with 10 and 20 GeV/e Protons, Parts I-V, Nucl. Inst. and Methods 32: 45.
7. R. L. Childers, C. D. Zerby, C. M. Fisher and R. H. Thomas, 1965, Measurement of the Nuclear Cascade at 10 GeV/c with Emulsions, Part III op. cit Ref. 6.

8. A. R. Smith, L. D. Stephens and R. H. Thomas, 1961, Dosimetry for Radiobiological Experiments, Health Physics, 32: 343 (1977).
9. A. R. Smith and R. H. Thomas, The Production of  $^{11}\text{C}$  by the Interaction of 375 MeV/amu  $\text{Ne}^{10+}$  ions with carbon, Nucl. Inst and Methods. 137: 459.
10. J. W. Patrick, L. D. Stephens, R. H. Thomas and L. S. Kelly, 1975, The Efficiency of  $^7\text{LiF}$  Thermoluminescent Dosimeters for Measuring 250 MeV/amu  $^6\text{C}$  ions, Health Physics 28: 614.
11. J. W. Patrick, L. D. Stephens, R. H. Thomas and L. S. Kelly, 1976, The Efficiency of  $^7\text{LiF}$  Thermoluminescent Dosimeters to High-LET particles, relative to  $^{60}\text{Co}$   $\gamma$ -rays, Health Physics 30: 295.
12. A. M. Henson and R. H. Thomas, 1978, Measurement of the Efficiency of  $^7\text{LiF}$  Thermoluminescent Dosimeters to Heavy Ions, Health Physics 34: 389 (1978).
13. J. W. Patrick, L. D. Stephens, R. H. Thomas and L. S. Kelly, 1975, The Design of an Experiment to Study Leukemogenesis in Mice Irradiated by Energetic Heavy Ions, Rad. Res. 64: 492.
14. L. S. Kelly, S. J. Daniels, and R. H. Thomas, 1977, Life Shortening and Leukemogenic Effects of a High-Energy Carbon-Ion Beam I: Irradiation of Young RF Mice, Lawrence Berkeley Laboratory internal report, HPN 92, September 1977 (unpublished).
15. L. S. Kelly and R. H. Thomas, 1977, Life Shortening and Leukemogenic Effects of a High-Energy Carbon-Ion Beam II: Irradiation of Middle-Aged RF Mice, Lawrence Berkeley Laboratory internal report, HPN 93 September 1977 (unpublished).
16. R. V. Griffith, D. E. Hankins, R. B. Gammage, L. Tommasino and R. V. Wheeler, 1979, Recent Developments in Personnel Neutron Dosimeters, A Review, Health Physics 36: 235.
17. K. Becker, 1973, "Solid State Dosimetry," CRC Press, Cleveland, OH.
18. J. Jasiak and T. Musialowicz, 1973, "Personnel Monitoring in Poland," in Proc. I.AE.A. Symp. on Neutron Monitoring for Radiation Protection Purposes, Vol. 1: 191, I.AE.A., Vienna.
19. K. Becker, 1973, Long Term Stability of Film, TLD and other Intergrating Dosimeters in Warm and Humid Climates, Oak Ridge National Laboratory Report ORNL-TM-4297.
20. P. N. Krishnamoorthy, G. Venkataramon, D. Singh and Dayashankar, 1973, "Comparison of Various Neutron Personnel Dosimeters" in Proc. Symp. Neutron Monitoring for Radiation Protection Purposes, Vol. 11., p. 343, IAEA, Vienna.
21. A. Knight, 1974, Fading of Proton Recoil Tracks in Nuclear Emulsions, Health Physics, 27: 606.
22. A. M. Sayed and E. Piesch, 1974, Study of the Latent Fading of the NTA film and Track Etching Detectors at Various Temperatures and Humidities, Kernforschungszentrum, Karlsruhe, Internal Report KFK-2032.

23. R. H. Thomas, 1973, "Neutron Dosimetry at High-Energy Particle Accelerators in Neutron Monitoring for Radiation Protection Purposes," Vol. I, p. 327, IAEA, Vienna.
24. H. W. Patterson et al., 1972, An Evaluation of the Potential of Thick Nuclear Emulsions for Use as a High Energy Neutron Personal Dosimeter, Health Physics Group, Lawrence Berkeley Laboratory Internal Report No. 160.
25. R. H. Thomas, 1973, Personnel Neutron Dosimetry Studies at the Lawrence Berkeley Laboratory, Lawrence Berkeley Laboratory Report LBL-2057.
26. H. W. Patterson and R. H. Thomas, 1973, Radiation Measurements, in "Accelerator Health Physics," Academic Press, New York.
27. R. L. Lehmann and O. M. Fekula, 1964, Energy Spectra of Stray Neutrons from the Bevatron, Nucleonics 22 (No. 11): 35.
28. R. Remy, 1965, Neutron Spectroscopy by the Use of Nuclear Stars from 20-300 MeV (M. S. Thesis) Lawrence Berkeley Laboratory Report UCRL-16325.
29. H. W. Patterson, H. Heckmann and J. T. Rotti, 1969, "New Measurements of Star Production in Nuclear Emulsions and Applications to High-Energy Neutron Spectroscopy," in Proc. Sec. Conference Acc. Dos. Stanford, California. Nov. 1969. USAEC Report - CONF-691101 p. 750.
30. W. S. Gilbert, et al., 1968, 1966 CERN-LRL-RHEL Shielding Experiment. Lawrence Berkeley Laboratory Report UCRL-17941.
31. A. H. Sullivan, 1969, "The Present Status of Instrumentation for Accelerator Health Physics," in Proc. 2nd Int. Conf. on Accelerator Dosimetry and Experience, Stanford, California, Nov. 1969, CONF-691101.
32. D. R. Perry, 1967, Neutron Dosimetry Methods and Experience on the 7 GeV Proton Synchrotron, Nimrod, in "Neutron Monitoring, Neutron Monitoring," Proc. Symp. Vienna, 1966, p. 355, IAEA, Vienna.
33. A. R. Smith, 1965, Threshold Detector Applications to Neutron Spectroscopy at the Berkeley Accelerators, in "Proc. First Symp. Acc. Rad. Dos." Brookhaven National Laboratory USAEC Report, CONF-651109, p 224.
34. A. R. Smith, 1965, Some Experimental Shielding Studies at the Bevatron, op. cit. ref. 33, p 365.
35. V. Perez-Mendez, 1979, Instrumentation--Active Detectors Lecture No. 9 in "Advances in Radiation, Protection and Dosimetry in Medicine," Course Proceedings, International School of Radiation Damage and Protection, Ettore Majorana Centre for Scientific Culture, Erice, Italy.
36. R. H. Thomas, 1979, Radiation Monitoring, Lecture No. 26, in Radiation Protection and Dosimetry in Medicine," Course Proceedings, International School of Radiation Damage and Protection, Ettore Majorana Centre for Scientific Culture, Erice, Italy.

37. R. L. Bramblett, R. I. Ewing, T. W. Bonner, 1960, A New Type of Spectrometer, Nucl. Instrum. Meth. 9 (1960); 1.
38. H. W. Patterson and R. H. Thomas, 1971, Experimental Shielding Studies--A Review, Particle Accelerators 2: 77.
39. J. T. Routti, 1969, "Mathematical Considerations of Determining Neutron Spectra from Activation Measurements," in Proc. Second Int. Conf. on Acc. Dos. Stanford, USAEC Report CONF 691101, p 494.
40. L. D. Stephens, J. B. McCaslin, A. R. Smith, R. H. Thomas, J. E. Hewitt, L. Hughes, 1978, Ames Collaborative Study of Cosmic Ray Neutrons, II Low and Mid-latitude Flights, Lawrence Berkeley Laboratory Report LBL-6738.
41. J. B. McCaslin, A. R. Smith, L. D. Stephens, R. H. Thomas, T. M. Jenkins, G. T. Warren and J. W. Baum, 1977, An Inter-comparison of Dosimetry Techniques in Radiation Fields at High-Energy Accelerators, Health Physics 33: 611.
42. H. de Staebler, 1979, Similarity of Shielding Problems at Electron and Proton Accelerators. op cit Ref. 33, p 429.
43. W. N. Hess, H. W. Patterson, R. W. Wallace, E. L. Chupp, 1959, The Cosmic Ray Neutron Energy Spectrum, Phys. Rev. 116: 445.
44. T. W. Armstrong, K. C. Chandler and J. Barish, 1972, Calculation of the Neutron Spectrum in the Earth's Atmosphere Produced by Galactic Cosmic Rays, Neutron Physics Division Annual Rep., ORNL-4800, p. 63.
45. A. R. Smith, 1974, Activation Element Monitoring for Mouse Irradiations (Lola Kelly Bevalac Run, 11/28/74), Lawrence Berkeley Laboratory, Health Physics Department Internal Note, HPN 21.
46. A. R. Smith and H. Wollenberg, 1966, A Low Background Counting Enclosure, Health Physics 12: 53.
47. A. R. Smith, 1974, Distribution of Fluorine-18 and Na-24 in Thick Aluminum Stack Irradiated in 380 MeV/N Neon Beam, Lawrence Berkeley Laboratory, Health Physics Department Internal Note.
48. C. A. Tobias, A. Chatterjee and A. R. Smith, 1971, Radioactive Fragmentation of  $N^{7+}$  Ion Beam Observed in a Beryllium Target, Physics Letters, 37A, a2.
49. A. R. Smith, 1975, Lawrence Berkeley Laboratory, Private communication.
50. Private Communication.
51. L. D. Stephens, R. H. Thomas and L. S. Kelly, 1976, A Measurement of the Average Energy Required to Create An Ion Pair in Nitrogen by 250 MeV/amu  $C^{6+}$  Ions, Phip. Med. Biol. 21: 570.
52. R. H. Thomas, J. T. Lyman, and T. M. de Castro, 1979, A Measurement of the Average Energy Required to Create an Ion Pair in Nitrogen by High-Energy Ions, Lawrence Berkeley Laboratory Report, LBL-6710, Rev. 2.

53. G. N. Whyte, 1963, Energy per Ion Pair for Charge Particle in Gases, Radiat. Res. 18: 265-271.
54. C. J. Bakker and E. Segre, 1961, Stopping Power and Energy Loss for Ion Pair Production for 300 MeV Protons, Phys Rev. 81: 489-492.
55. M. N. Verma, J. W. Baum and A. V. Kuhner, 1977, Radial dose, LET and w for  $^{16}\text{O}$  Ions in  $\text{N}_2$  and Tissue Equivalent Gases. Radiat. Res. 70: 511-518.
56. M. N. Varma, J. W. Baum and A. V. Kuhner, 1975, Experimental Determination of w. for Oxygen Ions in Nitrogen, Phys. Med. Biol. 20: 955.
57. K. Becker, 1973, "Solid State Dosimetry," CRC Press, Cleveland.
58. G. de Planque and T. F. Gesell, 1979, Second International Intercomparison of Environmental Dosimeters. Health Physics, 36: 221.
59. J. R. Cameron, N. Suntharlingham and G. N. Kenney, 1968, "Thermoluminescent Dosimetry," University of Wisconsin Press, Madison.
60. B. Jahnert, 1972, The Response of TLD-700 Thermoluminescent Dosimetry to Protons and Alpha Particles, Health Physics, 23: 112-115.
61. H. Grunder, ed., 1973, Heavy Ion Facilities and Heavy Ion Research at Lawrence Berkeley Laboratory, Lawrence Berkeley Laboratory Report LBL-2090.
62. E. Schopper, et al., 1972, Review on AgCl Crystals as Visual Detectors of Nuclear Particles, in Proc. 8th Int. Conf. on Nuclear Photography and Visual Detectors, Bucharest.
63. P. G. Stewart, 1968, Stopping Power and Range for Any Nucleus in the Specific Energy Interval 0.01 to 500 MeV/amu in Any Non-Gaseous Material, Lawrence Berkeley Laboratory Report, UCRL-18127.